

# Exploring Between the Extremes: Conversion-Dependent Kinetics of Phosphite-Modified Hydroformylation Catalysis

Christoph Kubis,<sup>[a, b]</sup> Detlef Selent,<sup>\*[a]</sup> Mathias Sawall,<sup>[c]</sup> Ralf Ludwig,<sup>[a, b]</sup>  
Klaus Neymeyr,<sup>[c]</sup> Wolfgang Baumann,<sup>[a]</sup> Robert Franke,<sup>[d, e]</sup> and Armin Börner<sup>[a, b]</sup>

**Abstract:** The kinetics of the hydroformylation of 3,3-dimethyl-1-butene with a rhodium monophosphite catalyst has been studied in detail. Time-dependent concentration profiles covering the entire olefin conversion range were derived from in situ high-pressure FTIR spectroscopic data for both, pure organic components and catalytic intermediates. These profiles fit to Michaelis–Menten-type kinetics with competitive and uncompetitive side reactions involved. The characteristics found for

the influence of the hydrogen concentration verify that the pre-equilibrium towards the catalyst substrate complex is not established. It has been proven experimentally that the hydrogenolysis of the intermediate acyl complex remains rate limiting even at high con-

versions when the rhodium hydride is the predominant resting state and the reaction is nearly of first order with respect to the olefin. Results from in situ FTIR and high-pressure (HP) NMR spectroscopy and from DFT calculations support the coordination of only one phosphite ligand in the dominating intermediates and a preferred axial position of the phosphite in the electronically saturated, trigonal bipyramidal (tbp)-structured acyl rhodium complex.

**Keywords:** density functional calculations • hydroformylation • in situ spectroscopy • kinetics • phosphites • rhodium

## Introduction

The hydroformylation of olefins with modified and also unmodified catalysts based on rhodium and cobalt is applied on a large industrial scale. It is one of the widely studied reactions in homogeneous catalysis.<sup>[1]</sup> This reaction has intensively stimulated the development of an in situ spectroscopic methodology in order to get detailed mechanistic information on catalytic cycles.<sup>[2]</sup> In situ FTIR spectroscopy has been proven a valuable tool for kinetic studies on unmodified homo- and heterodimetallic hydroformylation cata-

lysts.<sup>[3]</sup> Furthermore, it has been exemplified for rhodium-catalyzed hydroformylation that chemometric methods combined with an appropriate experimental design and in situ spectroscopy allow for a deep insight into the catalytical system under study.<sup>[4]</sup>

Hydroformylation is a typical catalytic multistep reaction. Our considerations in this paper are based on the dissociative mechanism as proposed by Wilkinson and co-workers for the Rh/PPh<sub>3</sub> catalytic system, and more recent results proving that bulky monophosphites tend to form tricarbonyl hydrido complexes ([HRh(CO)<sub>3</sub>L], see Scheme 1).<sup>[5]</sup>

The catalyst is represented by the 16-electron hydrido complex **2** resulting from carbon monoxide dissociation of the electronically saturated hydrido complex **1**. This equilibrium is competitive to olefin coordination at complex **2**. The latter elementary step is needed to open up the catalytic cycle by formation of the  $\pi$ -complex **3**. Hydride migration to the coordinated olefin affords the 16-electron *n*-alkyl complex **4**, or the corresponding *iso* derivative if hydride transfer occurs to the terminal olefin carbon atom. The coordination of CO is required to form the saturated alkyl complex **5**, which, by migratory insertion of carbon monoxide generates the 16-electron acyl intermediate **6**. This reactive intermediate can either coordinate carbon monoxide or react with hydrogen. With CO the 18-electron acyl complex **7** is formed, which is not capable of undergoing hydrogen activation. This substrate complex therefore represents a product of uncompetitive inhibition. Often complex **7** is populated sufficiently for a direct observation during catalysis.<sup>[3c,6]</sup> The nature of the hydrogen activation at intermediate **6** remains uncertain, despite efforts to study this reaction

[a] C. Kubis, Dr. D. Selent, Prof. R. Ludwig, Dr. W. Baumann, Prof. A. Börner  
Leibniz-Institut für Katalyse e.V. an der Universität Rostock  
Albert-Einstein-Strasse 29a, 18059 Rostock (Germany)  
Fax: (+49)381-128151169  
E-mail: detlef.selent@catalysis.de

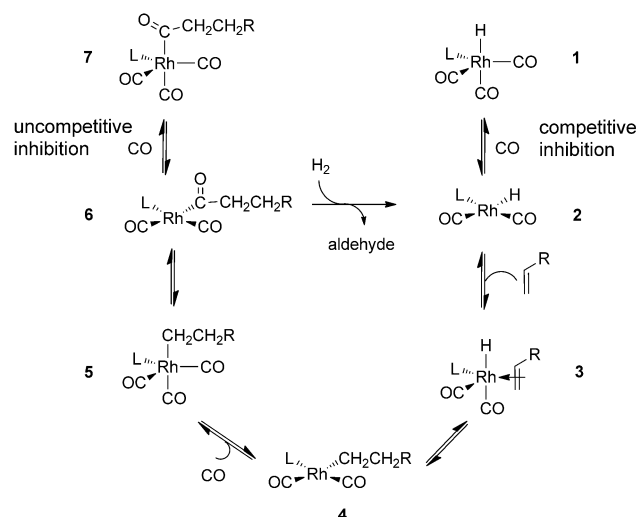
[b] C. Kubis, Prof. R. Ludwig, Prof. A. Börner  
Institut für Chemie, Universität Rostock  
Albert-Einstein-Strasse 3, 18059 Rostock (Germany)

[c] Dr. M. Sawall, Prof. K. Neymeyr  
Institut für Mathematik, Universität Rostock  
Ulmenstrasse 69, 18057 Rostock (Germany)

[d] Prof. R. Franke  
Evonik Industries AG  
Paul-Baumann-Strasse 1, 45772 Marl (Germany)

[e] Prof. R. Franke  
Lehrstuhl für Theoretische Chemie  
Ruhr-Universität Bochum  
44780 Bochum (Germany)

Supporting information for this article is available on the WWW under <http://dx.doi.org/10.1002/chem.201200603>.



Scheme 1. Simplified mechanism of the rhodium-catalyzed hydroformylation with the bulky monodentate ligand L. Only the pathway to the *n*-aldehyde is depicted.

with highly sensitive spectroscopic techniques.<sup>[7]</sup> Aldehyde elimination with regeneration of complex **1** may rather occur reductively from a rhodium(III) dihydrido complex intermediate than from a  $\eta^2$ -H<sub>2</sub> educt in a reaction related to sigma bond metathesis.<sup>[7d,8]</sup>

During modified rhodium catalysis, as products of the inhibitory side reactions, the only species detectable are the saturated complexes [HRh(CO)<sub>3</sub>L] (**1**) and [RC(O)Rh(CO)<sub>3</sub>L] (**7**) rather than the catalytically active 16-electron complexes.<sup>[9]</sup> The substrate used and the modifying ligand are known to affect the location of the rate-controlling step(s).<sup>[1a,10]</sup> Thus, hydroformylation of terminal olefins with monodentate bulky phosphites at high substrate-to-rhodium ratios is characterized by a nearly zero reaction order with respect to the olefin and the observation of the acyl complex **7** as the dominant catalytic species.<sup>[10d,f]</sup> With decreasing substrate concentration, there is a shift to a first-order reaction. We showed in a recent study that this is coupled with a subsequent decrease of the concentration of complex **7** from the beginning of the reaction, and the regeneration of the hydrido complex **1**.<sup>[11]</sup> Thus, with such catalysts only the initial rates obtained at high substrate concentrations are correlated in a linear fashion with the hydrogen concentration.<sup>[10e,f,12]</sup> A similar dependency will be observed with the pre-equilibrium established already at low acyl complex molar fractions. But, up to now, such case has not been reported for phosphite-modified rhodium catalysts. The saturation kinetics discussed here is typical for other cases in transition-metal catalysis, but has rarely been studied in a detailed manner.<sup>[13]</sup> Because there is a strong analogy to kinetic principles valid in enzyme catalysis, the respective mathematical treatment can be applied accordingly.<sup>[13–15]</sup>

In this paper, we present an extended study on the monophosphite-modified rhodium-catalyzed hydroformylation as a continuation of earlier work.<sup>[11]</sup> In situ FTIR spectroscopy

has been combined with DFT calculations to assign the structures of the rhodium complexes observed during the hydroformylation. We show that the kinetic behavior of the catalyst can be described conveniently by applying the Michaelis–Menten kinetics approach. Correlations between the rate of product formation and the concentration profiles for the observable organometallic species are presented that are valid for the entire conversion range. To the best of our knowledge, similar results have rarely been described before for such type of catalyst.<sup>[16]</sup>

## Results and Discussion

**Michaelis–Menten-type kinetics for hydroformylation:** Our treatment of the hydroformylation reaction follows the Christiansen formalism as has been detailed in reference [15a] and results in Equation (1). For the detailed derivation, which was made with the constraint that the concentration of carbon monoxide is constant, see the Supporting Information, SI-A. Established procedures are known for the formal handling of catalytic reaction cycles involving inhibitory side reactions, which also allow the rate equations obtained to be reduced to relations, which represent the experimentally observable kinetic behavior.<sup>[15a,d,17,18]</sup> The formalism used is based on the quasi-stationary approximation of respective intermediates, which leads to dependencies equivalent to those described by the Michaelis–Menten equation.

$$V = \frac{d[P]}{dt} = \frac{\left( \prod_{i=0}^{k-1} \lambda_{i,i+1} - \prod_{i=0}^{k-1} \lambda_{i+1,i} \right) [\text{Cat}]_0}{D + D_{00} \frac{[\text{CO}]}{K_{\text{inh},c}} + D_{jj} \frac{[\text{CO}]}{K_{\text{inh},uc}}} \rightarrow V = \frac{k_2 [\text{H}_2] [\text{Cat}]_0 [\text{S}]}{\frac{k_{-1} + k_2 [\text{H}_2]}{k_1} + [\text{S}]} \quad (1)$$

For each single experiment, the concentration of hydrogen can be considered constant and Equations (2a)–(2c) apply.

$$k_2^{\text{obs}} = k_2 [\text{H}_2] \quad (2a)$$

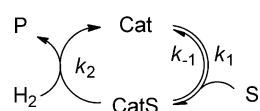
$$V_{\text{sat}} = k_2^{\text{obs}} [\text{Cat}]_0 \quad (2b)$$

$$K_m = \frac{k_{-1} + k_2^{\text{obs}}}{k_1} \quad (2c)$$

The rate  $V_{\text{sat}}$  represents the highest possible reaction rate at a physically not necessarily accessible substrate concentration where all of the catalyst is complexed by substrate, and  $K_m$  is the Michaelis constant as depicted in Equations (2) and (3).

$$V = \frac{V_{\text{sat}} [\text{S}]}{K_m + [\text{S}]} \quad (3)$$

Thus, hydroformylation can be considered to fit the simple Michaelis–Menten-type mechanism given in Scheme 2, with Cat and CatS representing pseudocompo-



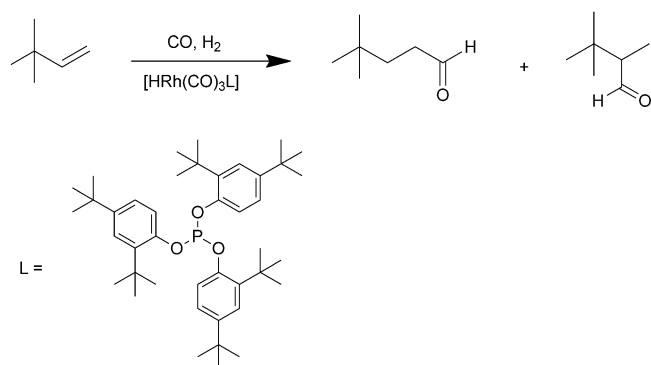
Scheme 2. Michaelis–Menten-type catalysis.

nents consisting of the 16- and 18-electron hydrido and acyl rhodium complexes, respectively, at a quasi-equilibrium.<sup>[15a,d]</sup> Consequently, all elementary steps preceding acyl complex formation are considered to belong to one reaction step.

We shall show that the quasi-stationarity of intermediates is not given for the Rh/monophosphite catalytic system under investigation. But with  $[\text{Cat}]_0 \ll [\text{S}]_0$  the Bodenstein approximation holds for nearly the entire conversion range and the experimental data can be analyzed by the Michaelis–Menten approach.

### Hydroformylation of 3,3-dimethyl-1-butene in *n*-hexane:

3,3-Dimethyl-1-butene as a substrate was converted with a rhodium/tri(2,4-di-*tert*-butylphenyl)phosphite (TDTBPP or L) catalyst at  $[\text{Rh}] = 0.3 \text{ mM}$ ,  $T = 30^\circ\text{C}$ ,  $p_{\text{CO}} = 1 \text{ MPa}$ ,  $p_{\text{H}_2} = 1 \text{ MPa}$ , see Scheme 3. As a change to our earlier study in cy-



Scheme 3. Hydroformylation of 3,3-dimethyl-1-butene with a rhodium/tri(2,4-di-*tert*-butylphenyl)phosphite catalyst.

clohexane, *n*-hexane was used as a solvent because the background subtraction required during the preprocessing of the FTIR spectroscopic data could be performed in a much more reliable manner. The olefin selected is not able to undergo double-bond isomerization, which would otherwise alter the kinetic behavior.

Before the substrate was added,  $[(\text{acac})\text{Rh}(\text{CO})_2]$  (*acac* = acetylacetonate anion) in the presence of twenty equivalents of TDTBPP was reacted to the pentacoordinate hydrido complex  $[\text{HRh}(\text{CO})_3\text{L}]$  under conditions intended for catalysis. Complete conversion to the hydride required 16 h at  $30^\circ\text{C}$ . The final IR spectrum shows the main component  $[\text{HRh}(\text{CO})_3\text{L}]$  with  $\tilde{\nu}(\text{CO}) = 2015, 2043, \text{ and } 2093 \text{ cm}^{-1}$  and contributions of a minor compound at  $\tilde{\nu}(\text{CO}) = 2028$  and  $2068 \text{ cm}^{-1}$ , attributed to the bisphosphite hydrido complex  $[\text{HRh}(\text{CO})_2\text{L}_2]$ .<sup>[5c,d]</sup> After addition of the olefin a slow hydroformylation reaction started without induction time, taking  $> 15 \text{ h}$  for full conversion.

The concentration profile of the aldehyde product, as determined by IR spectroscopy, did fit to that obtained by

GC.<sup>[19]</sup> The reaction proceeds highly chemoselective and with the same kinetics for both aldehyde products, 4,4-dimethylpentanal and 2,3,3-trimethylbutanal, with the latter isoaldehyde representing a constant 0.099 molar fraction over the whole conversion range. Therefore, in Figure 1 a the sum

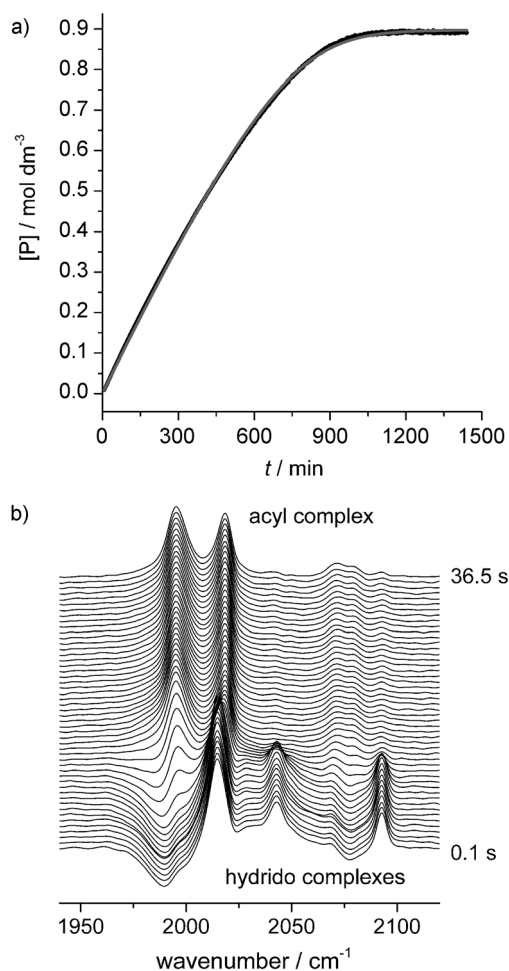


Figure 1. Hydroformylation of 3,3-dimethyl-1-butene. a) Concentration versus time plot of the sum of aldehydes (*n*+*iso*, black curve). Experimental data obtained from FTIR spectroscopy at the reference wavenumber  $\tilde{\nu} = 1765.1 \text{ cm}^{-1}$  to avoid nonlinearities of the absorption at the aldehyde carbonyl band maximum, compared to the regression curve (gray curve) from the numerically integrated Michaelis–Menten equation. b) Transient phase kinetics of acyl complex formation;  $[\text{HRh}(\text{CO})_3\text{L}]$  (main component):  $\tilde{\nu}(\text{CO}) = 2015, 2043, 2093 \text{ cm}^{-1}$ ,  $[\text{HRh}(\text{CO})_2\text{L}_2]$  (minor component)  $\tilde{\nu}(\text{CO}) = 2028, 2068 \text{ cm}^{-1}$ , acyl complex:  $\tilde{\nu}(\text{CO}) = 1995, 2019, 2072, \text{ and } 2079 \text{ cm}^{-1}$ . Conditions:  $[\text{Rh}] = 0.3$ ,  $[\text{TDTBPP}] = 6 \text{ mM}$ ;  $[\text{olefin}]_0 = 0.9 \text{ M}$ ;  $T = 30^\circ\text{C}$ ;  $p_{\text{CO}} = 1$ ,  $p_{\text{H}_2} = 1 \text{ MPa}$ ; solvent: *n*-hexane.

of aldehydes is used to illustrate the dynamics of the product formation. These experimental concentration versus time data of the aldehyde(s) were used for a nonlinear regression to compute the possible maximum rate  $V_{\text{sat}} = 1.52 \times 10^{-3} \text{ mol dm}^{-3} \text{ min}^{-1}$  (for  $[\text{CatS}] = [\text{Cat}]_0$ ) and  $K_m = 0.173 \text{ mol dm}^{-3}$  by numerical integration of the Michaelis–Menten equation [see Eq. (4)].

$$V = \frac{d[P]}{dt} = \frac{V_{\text{sat}}[S]}{K_m + [S]} = \frac{V_{\text{sat}}([S]_0 - [P])}{K_m + ([S]_0 - [P])} \quad (4)$$

To further support the result of the regression procedure, we simulated the Michaelis–Menten mechanism by solving the set of ordinary differential Equations (5a)–(5d).

$$\frac{d[S]}{dt} = -k_1[S][\text{Cat}] + k_{-1}[\text{CatS}] \quad (5a)$$

$$\frac{d[\text{Cat}]}{dt} = -k_1[S][\text{Cat}] + k_{-1}[\text{CatS}] + k_2^{\text{obs}}[\text{CatS}] \quad (5b)$$

$$\frac{d[\text{CatS}]}{dt} = k_1[S][\text{Cat}] - k_{-1}[\text{CatS}] - k_2^{\text{obs}}[\text{CatS}] \quad (5c)$$

$$\frac{d[P]}{dt} = k_2^{\text{obs}}[\text{CatS}] \quad (5d)$$

For that purpose, the known value of  $k_2^{\text{obs}}$  and the estimated values of  $k_1$  and  $k_{-1}$  obtained from a variation of the hydrogen pressure, which will be described below, have been used. Thus, evidence is given that the kinetic model implementing a steady-state approximation is also valid when the entire conversion range is taken into account.<sup>[20]</sup>

The initial rate  $V_0$  was calculated to  $1.27 \times 10^{-3} \text{ mol dm}^{-3} \text{ min}^{-1}$  according to Equation (6a).

$$V_0 = \frac{V_{\text{sat}}[S]_0}{K_m + [S]_0} \quad (6a)$$

$$\frac{V_0}{V_{\text{sat}}} = \frac{[\text{CatS}]}{[\text{Cat}] + [\text{CatS}]} \quad (6b)$$

As can be derived from Equation (6b), a 0.84 molar fraction of the catalyst resides in the intermediate acyl complex (CatS) at the beginning of the reaction. This does point to the fact, that the system does not operate under full saturation conditions at any time. An interesting result arised from a rapid scan measurement following the evolution of the reaction directly after olefin addition, see Figure 1 b. The formation of the acyl complex with  $\tilde{\nu}(\text{CO})=1995$ , 2019, 2072, and 2079  $\text{cm}^{-1}$  is fast, with most of the hydrido complex conversion taking place within a time span of five to seven seconds, after some delay, which probably is due to mixing phenomena. Unfortunately, the respective dynamics could not be followed precisely. The application of a stopped-flow methodology would be appropriate. However, it becomes clear that the formation of the acyl intermediate is much faster than the hydroformylation. The transient phase kinetics is therefore negligible.

**Improved spectroscopic analysis and concentration profiles of organometallic intermediates:** In a preceding paper we showed that the hydrido complex (Cat) does coexist with the acyl complex (CatS) over a wide conversion range. However, it has not been detected at a maximum substrate concentration.<sup>[11]</sup> By changing the solvent from cyclohexane to *n*-hexane and advanced background treatment, now better resolved FTIR spectra were obtained. Furthermore, the im-

plementation of solvent background subtraction into the spectra-decomposition routine allowed for a more precise reconstruction of the concentration profiles of the organometallic intermediates.

Figure 2a shows a spectrum stack covering the full conversion range. The first spectrum is obtained after catalyst preformation and represents an equilibrium mixture of the hydrido complexes  $[\text{HRh}(\text{CO})_3\text{L}]$  and  $[\text{HRh}(\text{CO})_2\text{L}_2]$  in a 13.3:1 ratio.<sup>[5c,d]</sup> After the addition of the olefin the acyl complex  $[\text{RC}(\text{O})\text{Rh}(\text{CO})_3\text{L}]$  is rapidly populated to the dominant intermediate. A certain fraction of the hydrido

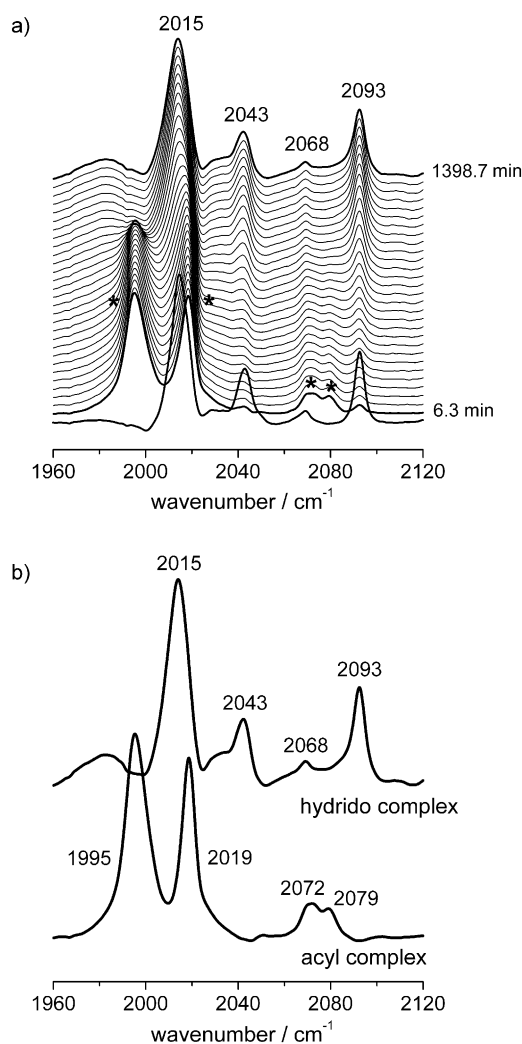


Figure 2. Hydroformylation of 3,3-dimethyl-1-butene. a) FTIR spectra after raw spectra treatment, see text for details. First spectrum: mixture of  $[\text{HRh}(\text{CO})_3\text{L}]$  ( $\tilde{\nu}(\text{CO})=2015$ , 2043, 2093  $\text{cm}^{-1}$ ) and  $[\text{HRh}(\text{CO})_2\text{L}_2]$  ( $\tilde{\nu}(\text{CO})=2028$ , 2068  $\text{cm}^{-1}$ , the low frequency band is obscured here) as obtained after catalyst preformation. Next spectrum, 6.3 min after addition of the olefin: The acyl complex  $[\text{RC}(\text{O})\text{Rh}(\text{CO})_3\text{L}]$  ( $\tilde{\nu}(\text{CO})=1995$ , 2019, and 2079  $\text{cm}^{-1}$ , indicated by asterisk) is dominant. For the origin of the band observed at  $\tilde{\nu}=2072 \text{ cm}^{-1}$ , see further results and discussion below. Background: *n*-hexane + conversion-dependent amount of substrate. b) Spectra of the acyl and hydrido complexes obtained by the application of the PCD software on the spectra sequence.<sup>[21]</sup> Conditions:  $[\text{Rh}]=0.3$ ,  $[\text{TDTBPP}]=6 \text{ mM}$ ;  $[\text{olefin}]_0=0.9 \text{ M}$ ;  $T=30 \text{ }^\circ\text{C}$ ;  $p_{\text{CO}}=1 \text{ MPa}$ ,  $p_{\text{H}_2}=1 \text{ MPa}$ ; solvent: *n*-hexane.

complex remains unreacted, which is in agreement with the evaluation of the product concentration profile by the kinetic model. With an increasing olefin consumption, the intensities of the bands for the acyl complex decrease, whereas those for the hydrido complex increase, finally resulting in a spectrum almost identical to that prior to the catalytic reaction. In Figure 2b the spectra of the hydride and the acyl complexes are given. Due to the very low rhodium concentration and the treatment of the conversion-dependent background required, artifacts were generated. See for example, the low frequency shoulder of the band located at  $\tilde{\nu}=2043\text{ cm}^{-1}$  in the spectrum of the hydrido complex. However, this did not hinder further analysis.

We want to describe briefly how the spectra shown in Figure 2 and the concentration profiles of the organometallic species as depicted in Figure 3a were obtained. The pure-component decomposition (PCD) software was applied.<sup>[21]</sup> The raw spectra required data preprocessing that took also into account the conversion dependency of the background.<sup>[22]</sup> Thus, it was possible to remove negative components, especially from a band at  $\tilde{\nu}=1990\text{ cm}^{-1}$  of the olefin, and to correct a strong drift of the zero line. The resulting series of spectra in the spectral interval of  $1960\text{--}2120\text{ cm}^{-1}$  is that shown in Figure 2a.

The concentration profiles of the acyl complex and the hydrido complex were obtained from the single-run spectra decomposition under the restriction of a constant rhodium concentration. Additionally, the set of ordinary differential equations for the Michaelis–Menten mechanism [Eq. (5a)–(5d)], was included as a regulative constraint. The kinetic constants  $k_1$ ,  $k_{-1}$ , and  $k_2^{\text{obs}}$  are usually determined in a way that the concentration profiles are fitted to such system of differential equations. As the spectral factorization by means of PCD is computed first this can be called an a-posteriori kinetic study. In contrast to this we used the error between a preliminary guess of the concentration profiles and their least-squares-fit to the system of ordinary differential equations as a further regularization of the PCD reconstruction functional. This approach can be considered as an a-priori kinetic analysis in which the structure of the differential equation regulates the result of the spectral factorization by PCD. Such kinetic regularization is known from the literature.<sup>[23]</sup> Numerical experiments that compare the results of an a-posteriori and an a-priori kinetic analysis clearly show an improved spectral reconstruction and a better kinetic modeling by means of the latter approach.<sup>[24]</sup> Figure 3a shows the results, namely the concentration profiles of the organometallic species together with those of the organic educt and the product, the latter as obtained from conventional FTIR analysis. Each of these profiles compares well to the corresponding least-squares-fit based on a Michaelis–Menten kinetic model. We further assumed that the concentration of the acyl complex reaches zero at full olefin conversion. The regression procedure did only allow for the determination of a distinct value of  $k_2^{\text{obs}}$ , whereas the values for  $k_1$  and  $k_{-1}$  for the pre-equilibrium remained numerically unstable. This uncertainty is probably caused by the fact

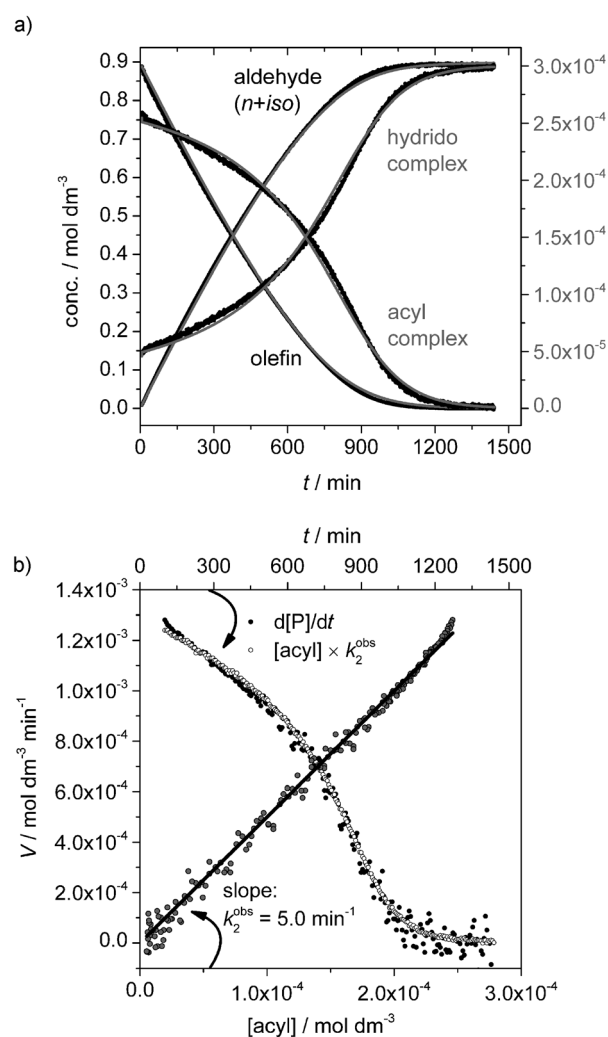


Figure 3. Hydroformylation of 3,3-dimethyl-1-butene. a) Concentration profiles of olefin and aldehydes as obtained conventionally from FTIR spectroscopy, and profiles of the organometallic components from PCD. The concentration range of the rhodium complexes is given by the right hand axis. Least-squares-fit from the Michaelis–Menten kinetic model (black curves: data, gray curves: regression). b) Comparison of the rate profile obtained from numerical differentiation of the aldehyde concentration profile (from the FTIR measurement, representing the 15% to full conversion range) with the numerical product of the rate constant  $k_2^{\text{obs}}$  with the acyl complex (CatS) concentration profile, and linear dependence between the rate of aldehyde formation and the acyl complex concentration. Conditions:  $[\text{Rh}]=0.3$ ,  $[\text{TDTBPP}]=6\text{ mM}$ ;  $[\text{olefin}]_0=0.9\text{ M}$ ;  $T=30\text{ }^\circ\text{C}$ ;  $p_{\text{CO}}=1$ ,  $p_{\text{H}_2}=1\text{ MPa}$ ; solvent: *n*-hexane.

that the formation of the acyl complex is fast with respect to mixing, thus preventing the recording of reliable spectra within approximately 2 min after olefin addition. The mathematical background is that the Hessian matrix of the reconstruction error functional is nearly singular in the  $k_1$  and  $k_{-1}$  directions. However, the  $K_m$  value, which is composed from the three rate constants, is in very good agreement with that from fitting the numerically integrated Michaelis–Menten equation to the profile of the aldehyde concentration (see Table 1). It is obvious that the investigated system with two observable organic and two catalytic components can be de-

Table 1. Kinetic constants obtained from different regression methods.

	System of ordinary differential equations, <sup>[a]</sup> PCD → [S], [Cat], [CatS], [P]	MM-equation, <sup>[b]</sup> FTIR + GC → [P]
$k_2^{\text{obs}}$ [min <sup>-1</sup> ]	5.00	5.05
$V_{\text{sat}}$ [mol dm <sup>-3</sup> min <sup>-1</sup> ]	$1.51 \times 10^{-3}$	$1.52 \times 10^{-3}$
$K_m$ [mol dm <sup>-3</sup> ]	0.179	0.173

[a] Integration/regression results from fitting the numerically integrated system of ordinary differential equations of the Michaelis–Menten mechanism [Eqs. (5a)–(5d)] to the four observable concentration profiles, see Figure 3 a. [b] Integration/regression results from fitting the numerically integrated Michaelis–Menten equation [Eq. (4)] to the product concentration profile, see Figure 1 a.

scribed by a Michaelis–Menten-type kinetics over the full conversion range.

Furthermore, Equation (5d) defines that the rate of product formation is linearly correlated with the concentration of the catalyst substrate complex. The expected result, therefore, is getting identical plots when comparing the rate profile of aldehyde formation with the profile obtained from the numerical product of the rate constant  $k_2^{\text{obs}}$  and the concentration of the intermediate acyl complex or alternatively from the numerical product of  $V_{\text{sat}}$  and the molar fraction of the same acyl complex. The plots given in Figure 3 b confirm such a linear correlation, which has been found also for unmodified hydroformylation catalysis.<sup>[3c,6a]</sup> By this relation it is obvious that the rate of product formation is limited by the hydrogenolytic step of the mechanism over the entire conversion range, which is also the rate-controlling step at high substrate concentrations, where  $[S] \gg K_m$ . In the region of the reaction where  $[S] \ll K_m$ , the free catalyst (Cat) is the predominant complex and the rate constant is a composed pseudo-first-order one. Therefore, in principle no step can be assigned as the rate-controlling step.<sup>[13,25]</sup>

### Influence of the hydrogen concentration on the rate and on the concentration profiles

**Characterization of the pre-equilibrium:** The good agreement between the Michaelis–Menten kinetic model applied here and the experimentally observed dependency of the rate of product formation on substrate concentration prompted us to study the influence of the concentration of the co-substrate hydrogen in more detail. Equations (1) and (2) indicate that the hydrogen concentration will influence the rate characteristically and also the product concentration profile. The pseudo constant  $k_2^{\text{obs}}$  is, besides  $K_m$ , a directly accessible physical quantity obtained by the integration/regression procedure. Furthermore, changing the hydrogen concentration will set a new balance between the concentrations of Cat and CatS at any distinct point of olefin conversion, thus also altering the concentration profiles for these intermediates.

A set of experiments was performed with different hydrogen partial pressures in the range between 0.2 and 3.8 MPa  $H_2$  and a constant  $p_{CO}=1$  MPa, with all other parameters

unchanged. For the calculation of the molar concentrations of hydrogen in *n*-hexane at 30 °C we used literature data.<sup>[26]</sup> It can be seen from Figure 4 that there is indeed a clear linear correlation between the values of  $k_2^{\text{obs}}$  and the hydro-

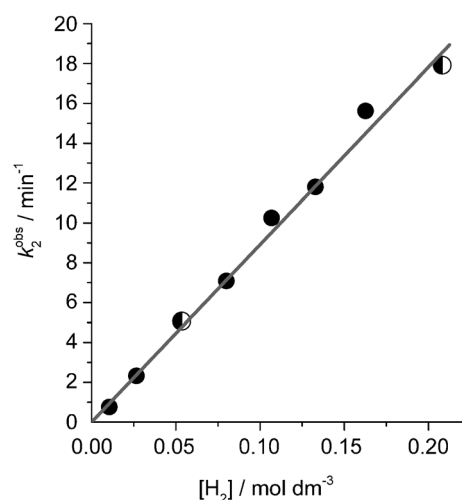


Figure 4. Hydroformylation of 3,3-dimethyl-1-butene. Influence of the hydrogen concentration on  $k_2^{\text{obs}}$ . Conditions: [Rh]=0.3, [TDTBPP]=6 mM; [olefin]<sub>0</sub>=0.9 M;  $T=30$  °C;  $p_{CO}=1$  MPa; solvent: *n*-hexane. For data on hydrogen concentration in solution see Table 2.<sup>[26]</sup> Repetition experiments are indicated by half-filled circles.

gen concentration in solution; respective data are given in Table 2. The plot of  $\ln(k_2^{\text{obs}})$  versus  $\ln([H_2])$  verifies the linear relationship, a partial reaction order with respect to the hydrogen concentration of 1.05 is obtained.

Table 2. Head space hydrogen pressures applied, effective hydrogen concentration in solution as calculated from data given in reference [26], and constants  $k_2^{\text{obs}}$ .

$p_{H_2}$ [MPa]	Conc. $H_2$ [mol dm <sup>-3</sup> ]	$k_2^{\text{obs}}$ [min <sup>-1</sup> ] <sup>[b]</sup>	$k_2^{\text{obs}}$ [min <sup>-1</sup> ] <sup>[c]</sup>
0.20	0.011	0.76	0.74
0.50	0.027	2.32	2.08
1.01	0.054	5.05	5.00
1.00 <sup>[a]</sup>	0.053	5.07	5.02
1.49	0.080	7.09	7.21
1.98	0.107	10.25	10.31
2.55	0.133	11.80	12.81
2.99	0.163	15.63	16.27
3.81	0.209	17.89	18.98
3.81 <sup>[a]</sup>	0.208	17.91	19.18

[a] Repetition experiments. [b] Values from Figure 4. [c] Values from Figure 5.

The values of  $k_2^{\text{obs}}$  were obtained from  $V_{\text{sat}}$  after fitting the numerically integrated Michaelis–Menten equation to the aldehyde profiles.<sup>[27]</sup> A value of 89.1 dm<sup>3</sup> mol<sup>-1</sup> min<sup>-1</sup> for  $k_2$  is directly derived from the slope. Two additional experiments performed at 1 and 3.8 MPa hydrogen pressure, respectively, verify the reproducibility of the results.

For all experiments a linear relationship is also found for different hydrogen concentrations when the rate of product

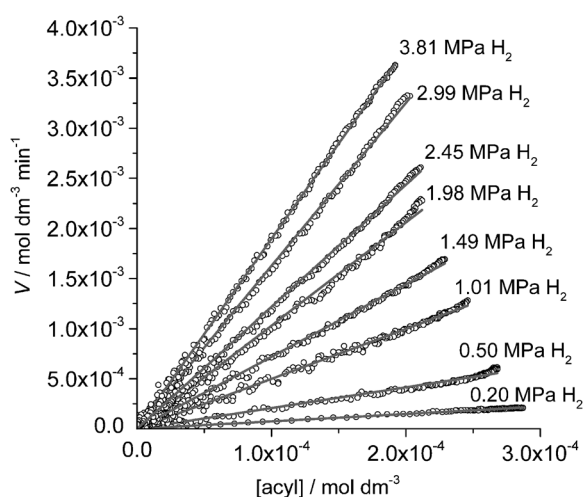


Figure 5. Correlation of the product formation rate with the concentration of the intermediate acyl complex at different hydrogen head space partial pressures for the hydroformylation of 3,3-dimethyl-1-butene. Rates were calculated by numerical differentiation of the aldehyde concentration curve after smoothing. Conditions:  $[Rh]=0.3$ ,  $[TDTBPP]=6$  mM;  $[olefin]_0=0.9$  M;  $T=30^\circ\text{C}$ ;  $p_{CO}=1$  MPa; solvent: *n*-hexane.

formation is plotted against the concentration of the intermediate acyl complex obtained from PCD (see Figure 5). Head space pressures of hydrogen are given, because they correlate linearly with the solution concentrations of  $\text{H}_2$  within the pressure range applied (see Table 2). The slopes of those straight lines represent the respective  $k_2^{\text{obs}}$  values, which are listed in Table 2. By linear regression of the data set  $k_2^{\text{obs}}$  values versus hydrogen concentration, the constant  $k_2$  was calculated to  $93.3 \text{ dm}^3 \text{ mol}^{-1} \text{ min}^{-1}$  which is in good agreement with the former value of  $89.1 \text{ dm}^3 \text{ mol}^{-1} \text{ min}^{-1}$ .

The observed first-order dependency of the product formation rate on the hydrogen concentration is strictly only to be expected when one analyses the values of  $k_2^{\text{obs}}$  versus the hydrogen concentrations or when the pre-equilibrium is established. Then, a first-order dependence is observed also by using initial rates, independent from the catalyst saturation. We will show below that the pre-equilibrium, which is part of the Michaelis–Menten-type mechanism depicted in Scheme 2, is not established and therefore the first case is relevant for our reaction.

The first-order dependency illustrated in Figure 4 corresponds to the limiting situation where  $[S] \gg K_m$  and all catalytic material is in the form of the acyl complex and the rate is determined by  $k_2^{\text{obs}}$ . The  $K_m$  constant, as given with Equations (2) and (3), which do also contain the hydrogen concentration, then is negligible, thus the substrate concentration is eliminated from the equation. However when one analyses the dependency of the initial rates from the hydrogen partial pressure for the case where  $[S]$  is in the order of magnitude of  $K_m$  the latter is not negligible and the substrate concentration cannot be eliminated. This results in a broken order with respect to the hydrogen concentration, which will show a shift, depending on the (initial) substrate concentration.

To check this point we calculated the initial rates by using Equation (6a) with  $V_{\text{sat}}$  and  $K_m$  obtained from our experiments and arbitrarily chosen initial substrate concentrations. With these initial rates the observable partial reaction order with respect to the hydrogen concentration was obtained from the slope of a respective double logarithmic plot  $\ln(V_0)$  versus  $\ln([H_2])$ . It can be seen from Figure 6 that the reac-

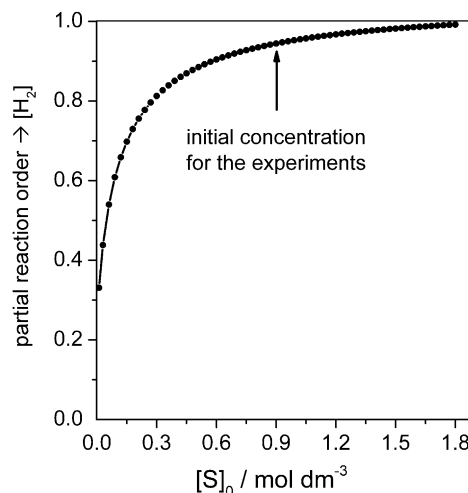


Figure 6. Partial reaction order with respect to the hydrogen concentration for different initial substrate concentrations for the hydroformylation of 3,3-dimethyl-1-butene. The calculation is based on the experimentally determined constants  $V_{\text{sat}}$  and  $K_m$  and Equation (6a).

tion under study is of nearly first order with respect to the hydrogen concentration at the starting point of the reactions with high olefin concentrations applied, but subsequently decreases with olefin consumption. Such broken order has indeed been found for other hydroformylation catalysts.<sup>[6f]</sup>

From the definition of  $K_m$  in Equation (2c), an information concerning the establishment of the pre-equilibrium can be obtained by variation of the hydrogen concentration. In the case of an established pre-equilibrium with  $k_{-1} \gg k_2[H_2]$ , Equation (7a) is valid.<sup>[13]</sup>

$$K_m = \frac{k_{-1}}{k_1} = \frac{1}{K} \quad (7a)$$

$$K_m = \frac{k_{-1}}{k_1} + \frac{1}{k_1} k_2 [H_2] \quad (7b)$$

Under these conditions, the constant  $K_m$  should be independent from the hydrogen concentration. On the other hand, when the pre-equilibrium is not established a linear dependence of  $K_m$  on  $[H_2]$  is expected. The constants  $k_1$  and  $k_{-1}$  can then be estimated from a plot of  $K_m$  versus  $k_2[H_2] = k_2^{\text{obs}}$  [Eq. (7b)] (see Figure 7 and Table 3).

There is a significant dependence of  $K_m$  on  $k_2^{\text{obs}}$ . Therefore, the pre-equilibrium is not established. The relation seems to be linear, as expected, with a deviation for the first data point that originates from the experiment at 0.2 MPa of

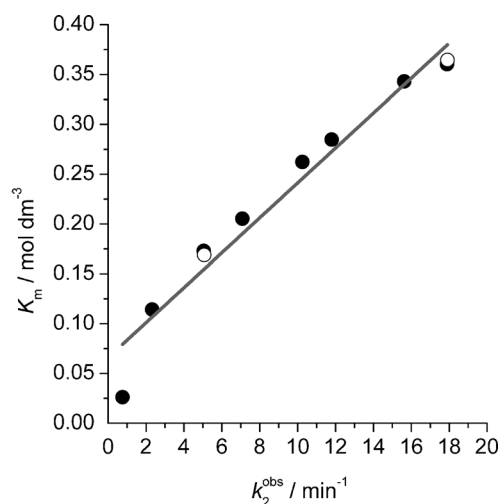


Figure 7. Plot of the Michaelis-Menten constant  $K_m$  versus  $k_2^{\text{obs}}$ , for the hydroformylation of 3,3-dimethyl-1-butene at different hydrogen partial pressures. Conditions:  $[\text{Rh}] = 0.3$ ,  $[\text{TDTBPP}] = 6 \text{ mM}$ ;  $[\text{olefin}]_0 = 0.9 \text{ M}$ ;  $T = 30^\circ\text{C}$ ;  $p_{\text{CO}} = 1 \text{ MPa}$ ; solvent: *n*-hexane. Open circles represent repetition experiments.

Table 3. Dependency of the Michaelis constant  $K_m$  on the hydrogen partial pressure.

$p_{\text{H}_2}$ [MPa]	$K_m$ [mol dm <sup>-3</sup> ]
0.20	0.03
0.50	0.11
1.01	0.17
1.00 <sup>[a]</sup>	0.17
1.49	0.21
1.98	0.26
2.55	0.28
2.99	0.34
3.81	0.36
3.81 <sup>[a]</sup>	0.36

[a] Repetition experiments.

hydrogen. At such low head space pressures of hydrogen, the determination of  $K_m$  is more difficult because the corresponding small amounts of hydrogen present in solution can lead to high molar fractions of the acyl complex also at low substrate concentrations.

Constants obtained by taking all data points into account were  $k_1 = 57.1 \text{ dm}^3 \text{ mol}^{-1} \text{ min}^{-1}$  and  $k_{-1} = 3.8 \text{ min}^{-1}$ . It is evident that  $k_{-1}$  is of similar magnitude, compared to  $k_2^{\text{obs}}$  (see Table 2). Therefore, a derivation of the rate equations based on the quasi-equilibrium approximation is not valid for this reaction system but a steady-state approach is suitable!

The results described above show, that the hydrogen concentration has a deciding influence on the behavior of the catalytic system under study. An impressive tool for illustrating the consequences of the variation of  $[\text{H}_2]$  are the concentration profiles, which include pure organic components but also the observable organometallic intermediates. Such profile sets have been determined for all experiments of the variation of the hydrogen partial pressure series. Each profile was reconstructed for the entire olefin conversion

range as described above. Figure 8 shows two selected sets of profiles, which were obtained at 0.2 and 3.81 MPa, respectively, of hydrogen partial pressure.<sup>[28]</sup> For comparison and verification, each individual profile is accompanied by the result of a simultaneous integration/regression of the set of ordinary differential Equations (5a)–(5d).

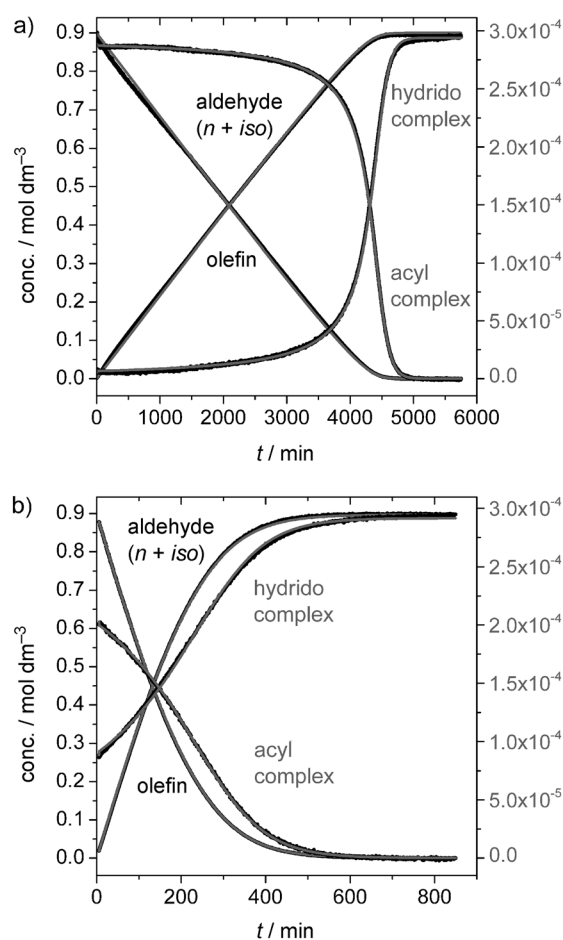


Figure 8. Influence of the hydrogen pressure ( $p_{\text{H}_2} = 0.20$  (a) or 3.81 MPa (b)). Concentration profiles and results of simultaneous integration/regression for the reactants (olefin), products (aldehyde sum), and observable rhodium complexes (right-hand axis) during the hydroformylation of 3,3-dimethyl-1-butene. Conditions:  $[\text{Rh}] = 0.3$ ,  $[\text{TDTBPP}] = 6 \text{ mM}$ ;  $[\text{olefin}]_0 = 0.9 \text{ M}$ ;  $T = 30^\circ\text{C}$ ;  $p_{\text{CO}} = 1 \text{ MPa}$ ; solvent: *n*-hexane (black curves: data, gray curves: regression).

The profile set obtained for 0.2 MPa hydrogen pressure shows the acyl rhodium complex to dominate over the hydrido complex until  $> 90\%$  of conversion, with a nearly zero reaction order with respect to the olefin observed. This reaction took approximately 4500 min for completion. In contrast, the acyl complex is quickly depopulated at 3.81 MPa of  $\text{H}_2$  and a much faster aldehyde production takes place. The pressure-dependent initial concentrations of the acyl complex clearly indicate also that the pre-equilibrium is not established.

## Further investigations on the intermediates

**The hydrido complexes:** After catalyst preformation two hydrides,  $[\text{HRh}(\text{CO})_3\text{L}]$  and  $[\text{HRh}(\text{CO})_2\text{L}_2]$ , are present as potentially catalytically active species with the latter being the minor component. Because it was not possible to determine the exact molar fraction of that complex from the FTIR spectra taken at  $p_{\text{CO}}=p_{\text{H}_2}=1$  MPa, we performed a systematic variation of the CO partial pressure at a constant hydrogen partial pressure of 1 MPa and the same Rh/P ratio of 20 as has been applied for the catalytic batches. At a very low CO partial pressure of approximately  $10^{-3}$  MPa, only the vibrational bands of pure  $[\text{HRh}(\text{CO})_2\text{L}_2]$  are observable (see Figure 9).

We used the ratio of the peak areas of this hydrido complex band at  $\tilde{\nu}=2068$   $\text{cm}^{-1}$  and the band at  $\tilde{\nu}=1740$   $\text{cm}^{-1}$  of an internal reference (see the Experimental Section for further quantification). Figure 9 illustrates how the fractions of the complex depend on the CO partial pressure. There is some variance in the data due to the low rhodium concentration of 0.3 mM and the need for background subtraction. As expected from the corresponding mass action law, the fraction of the bisligand hydrido complex shows an inverse relation to the partial pressure of carbon monoxide. By least-squares fitting an equilibrium constant  $K=1.7$  has been determined for the substitution reaction depicted in Scheme 4. From these data a significant mole fraction of 0.07 was calculated for the standard carbon monoxide pressure of 1 MPa.

We assume that  $[\text{HRh}(\text{CO})_2\text{L}_2]$  is part of the pseudocomponent consisting of quasi-equilibrated hydrido complexes, and that any ligand exchange involving TDTBPP and CO required to form the intermediate acyl rhodium complex is fast.



Scheme 4. Equilibrium between the hydrido rhodium complexes formed with tri(2,4-di-*tert*-butylphenyl)phosphite.

Earlier work did not consistently address the question of the structure of the rhodium hydrido carbonyl complexes formed with TDTBPP. This prompted us to perform DFT calculations on molecules containing the actual phosphite ligand. Because spectroscopy will not always allow directly for a proper structural assignment of hardly isolable intermediates, a comparison of experimental FTIR spectra with such obtained from DFT calculations of a model compound can help with identification.<sup>[30]</sup>

Geometry optimization and frequency calculations were carried out for both isomers with an axially (*a*) and an equatorially (*e*) coordinated phosphite in  $[\text{HRh}(\text{CO})_3\text{L}]$ , as well as for the *e,e* and *e,a* isomers of  $[\text{HRh}(\text{CO})_2\text{L}_2]$ . The calculated frequencies shown in Figure 10 were not scaled, therefore shifts in the wavenumbers between the calculated and the experimental vibrational spectra naturally exist. This can

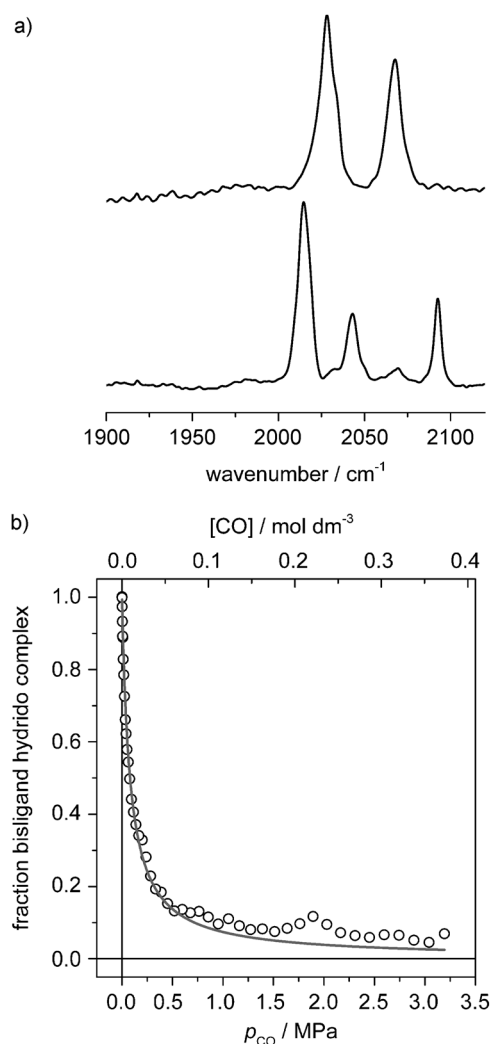


Figure 9. a) Experimental FTIR spectrum of the pure bisligand hydrido complex,  $\tilde{\nu}(\text{CO})=2028$  and  $2068$   $\text{cm}^{-1}$  at about  $p_{\text{CO}}=10^{-3}/p_{\text{H}_2}=1$  MPa (upper trace). Spectrum of  $[\text{HRh}(\text{CO})_3\text{L}]$  at the experimental standard partial pressures,  $p_{\text{CO}}=p_{\text{H}_2}=1$  MPa (lower trace). b) Fraction of  $[\text{HRh}(\text{CO})_2\text{L}_2]$  in dependence on the partial pressure of CO.<sup>[29]</sup> Experimental data according to the internal reference and fit according to  $[\text{HRh}(\text{CO})_2\text{L}_2]/[\text{Rh}]_0=K[\text{L}]/(K[\text{L}]+[\text{CO}])$ . All measurements performed in *n*-hexane, with  $[\text{Rh}]=0.3$  and  $[\text{TDTBPP}]=6$  mM.

clearly be seen for *e*- $[\text{HRh}(\text{CO})_3\text{L}]$ , where the spectrum from DFT is red shifted by approximately  $50$   $\text{cm}^{-1}$ , but the band pattern obtained compares well to the experimental one.

For  $[\text{HRh}(\text{CO})_2\text{L}_2]$ , a bisequatorial phosphite arrangement can be deduced. The calculations predict a band at  $\tilde{\nu}=1950$   $\text{cm}^{-1}$  originating from a stretching vibration of the Rh–H bond, which, probably due to low intensity and solvent effects, has not been detected during the experiment.

**The acyl complex:** The acyl rhodium complex formed in the intermediate step of carbon monoxide insertion is not only important for supporting the mechanistic rationale proposed for the hydroformylation reaction. This complex represents

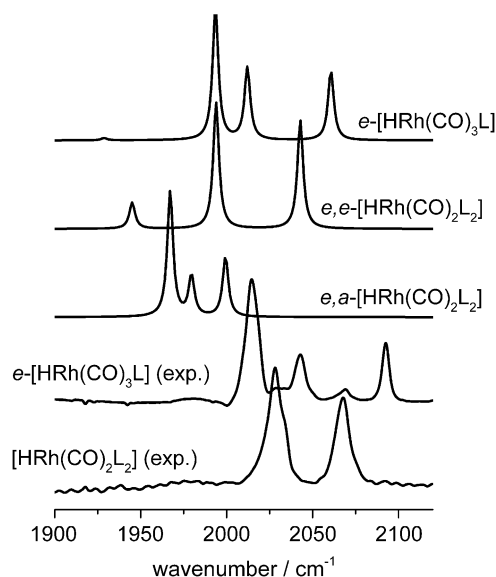


Figure 10. Comparison of experimental (two lower traces) spectra and spectra from DFT calculations of the rhodium hydride complexes formed with tri(2,4-di-*tert*-butylphenyl)phosphite. For optimized geometries see the Supporting Information.

the only component of the catalytic cycle that is detectable after olefin activation and before reformation of Cat. It therefore justifies a demand that is essential for the kinetic formalism applied here. Spectroscopic evidence for the formation of an acyl complex formed during the hydroformylation of 1-octene has been provided for a Rh/tri(2-*tert*-butyl-4-methylphenyl)phosphite catalyst. The authors succeeded in detecting a band at  $\tilde{\nu}=1690\text{ cm}^{-1}$  of the rhodium-bound acyl moiety by rapid scan technique before it was overlaid with the band of the strongly absorbing aldehyde group.<sup>[10d]</sup>

In our experiments, we could not observe a band at similar wavenumbers probably because of the low rhodium concentration of 0.3 mM applied. New measurements were therefore done at  $[\text{Rh}]=1.24\text{ mM}$ . To further stabilize the acyl complex, we adjusted the partial pressures to  $p_{\text{CO}}=4.65$  and  $p_{\text{H}_2}=0.2\text{ MPa}$ . Interestingly, the preformation of the hydrido complexes is now accompanied by a side reaction. Bands for bridging CO groups at  $\tilde{\nu}=1814$  and  $1835\text{ cm}^{-1}$  and further bands at  $\tilde{\nu}=2032$  and  $2049\text{ cm}^{-1}$  are observed, which we assign to dimeric  $\text{Rh}^0$  complexes. After the addition of the olefin, the hydrido complex instantly is converted to the acyl complex, whereas the dimer disappears in a slower reaction that takes 10 min. It also does react to the acyl complex, without any further intermediate observable. The modified reaction conditions allowed for the observation of an acyl carbonyl band, which is located at  $\tilde{\nu}=1690\text{ cm}^{-1}$ . This band gained intensity simultaneously with the known bands at  $\tilde{\nu}=1995$ , 2019, 2072, and  $2079\text{ cm}^{-1}$  (see Figure 11). The band at  $\tilde{\nu}=2072\text{ cm}^{-1}$  has not been observed earlier with the same reaction studied in cyclohexane solvent. Thus, the change of the methodology applied for better spectroscopic identification. Consequently, the application of a semi-

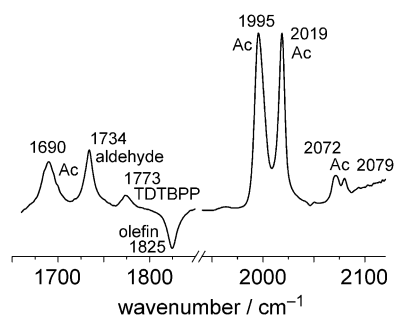


Figure 11. Hydroformylation of 3,3-dimethyl-1-butene at  $30^\circ\text{C}$  in *n*-hexane at  $p_{\text{CO}}=4.65$  and  $p_{\text{H}_2}=0.2\text{ MPa}$ ;  $[\text{Rh}]=1.24\text{ mM}$ ; TDTBPP/Rh=20;  $[\text{olefin}]_0=0.9\text{ M}$ . FTIR spectra of the carbonyl region taken 10 min after olefin addition to the solution of preformed catalyst. Ac=acyl complex  $[\text{C}_6\text{H}_{13}\text{C}(\text{O})\text{Rh}(\text{CO})_3(\text{TDTBPP})]$  (for an explanation of the band pattern see text); aldehyde=4,4-dimethylpentanal and 2,3,3-trimethylbutanal. The drop of the base line at  $\tilde{\nu}=1825\text{ cm}^{-1}$  originates from the subtraction of olefin from the background consisting of *n*-hexane and 3,3-dimethyl-1-butene.

batch methodology should further enhance the reliability of such spectroscopic work. We partly followed this approach by monitoring the spectra with a variety of carbon monoxide pressures ranging from 0.2 to 4.7 MPa, and also by changing the TDTBPP/Rh ratio. To reduce background correction problems arising from extended olefin consumption,  $[\text{Rh}]$  was set back to 0.3 mM. This also slowed down all reactions enough to perform the IR spectroscopic measurements within a 5% initial conversion range. The results are shown in Figure 12. When compared to Figure 11, no change within the spectral region of terminal carbonyls is observed. The band in question at  $\tilde{\nu}=2072\text{ cm}^{-1}$  does resist the pressure changes, and also a reduced concentration of the monophosphite has no effect. We conclude, that the spectrum recorded is indeed that of  $[\text{C}_6\text{H}_{13}\text{C}(\text{O})\text{Rh}(\text{CO})_3(\text{TDTBPP})]$  and that this acyl complex, in contrast to the results obtained for the hydrido complexes, is not in equilibrium to a detectable amount with the bisphosphite derivative  $[\text{C}_6\text{H}_{13}\text{C}(\text{O})\text{Rh}(\text{CO})_2(\text{TDTBPP})_2]$ .

One of the questions remaining is that of the structure of  $[\text{C}_6\text{H}_{13}\text{C}(\text{O})\text{Rh}(\text{CO})_3(\text{TDTBPP})]$ . An equatorial coordination of the structurally comparable tri(2-*tert*-butyl-4-methylphenyl)phosphite is discussed in the literature, with the axial positions of the trigonal bipyramidal (tbp)-structured molecule accommodated by the acyl fragment and a carbon monoxide ligand, respectively.<sup>[10d]</sup> For such geometry, we expect a similar spectral pattern in the terminal carbonyl region as is observed for the hydrido complex  $e\text{-}[\text{HRh}(\text{CO})_3\text{L}]$ . For the TDTBPP ligand used in this study, such similarity is not given. The spectrum of the corresponding acyl complex compares well to that of matrix-isolated acyl complexes of rhodium and more stable acyl derivatives of cobalt, containing triphenylphosphine.<sup>[6d,31]</sup> Thus, a structure with an axially coordinated phosphite is probably given. We performed DFT calculations as well as high-pressure (HP) NMR spectroscopic investigations to verify this hypothesis. For the calculations the actual acyl moiety  $(\text{CH}_3)_3\text{CCH}_2\text{CH}_2\text{C}(\text{O})$ , and

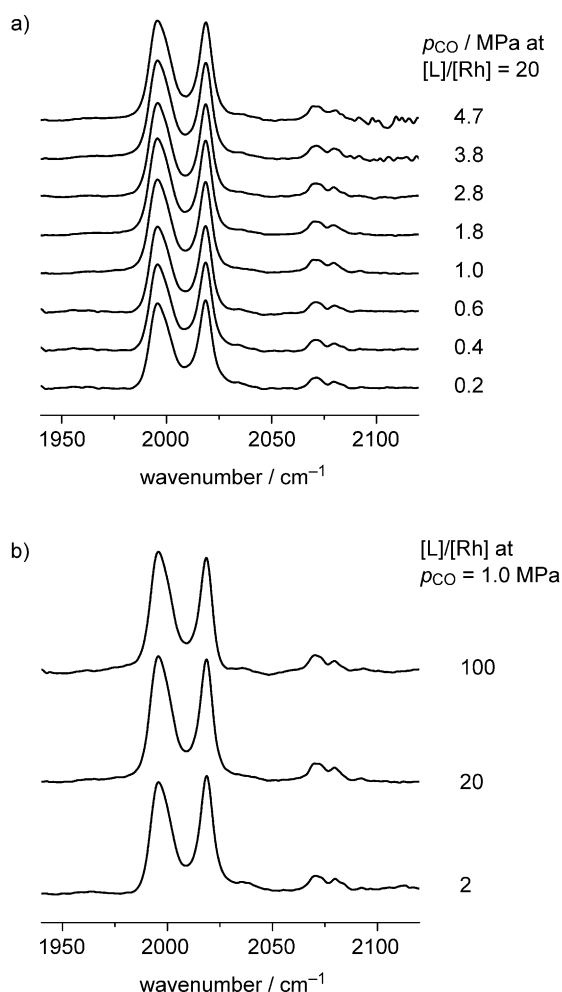


Figure 12. Hydroformylation of 3,3-dimethyl-1-butene at 30°C in *n*-hexane,  $[\text{Rh}] = 0.3 \text{ mM}$ ,  $[\text{olefin}]_0 = 0.9 \text{ M}$ . FTIR spectra of the acyl complex taken within a 5% olefin conversion range at a) different carbon monoxide partial pressures and b) different ratios of TDTBPP/Rh. Background correction involves olefin and *n*-hexane.

a structurally intact TDTBPP ligand were used. The result is shown in Figure 13, which compares the experimentally obtained FTIR spectrum of the acyl complex with those obtained from DFT calculations for both isomers. There is a good agreement of the spectral pattern between the experiment and the calculated spectrum representing a molecule with the phosphite coordinated in an axial position. Frequency analysis revealed, that both intense bands at  $\tilde{\nu} = 1995$  and  $2019 \text{ cm}^{-1}$  represent asymmetric stretching vibrations. The splitting of these terminal  $\nu(\text{CO})$  bands can be attributed to the carbonyl group of the acyl. Weinhold's NBO analysis shows that the oxygen lone pairs of the three CO ligands can donate charge into the corresponding Rh–C(O) anti bonds to different extent.<sup>[32]</sup> This leads to a lengthening of the Rh–C(O) bond of about  $0.025 \text{ \AA}$  and a shortening of the corresponding C–O bond ( $0.005 \text{ \AA}$ ) for the ligand that is neighbored to the carbonyl group of the acyl. This results in weaker coupling for one of the asymmetric vibrational modes of the CO ligands. The degeneracy of both asymmet-

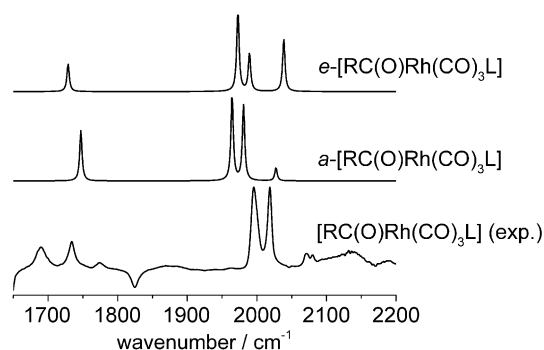


Figure 13. Experimentally observed FTIR spectrum of the acyl complex  $[\text{C}_6\text{H}_{13}\text{C}(\text{O})\text{Rh}(\text{CO})_3(\text{TDTBPP})]$  and the respective spectra obtained from DFT calculations for the phosphite ligand coordinated in an axial or equatorial position. For optimized geometries see the Supporting Information.

ric vibrational modes as present for a  $C_{3v}$  point group is here cancelled and one frequency is shifted to the red of about  $16 \text{ cm}^{-1}$ . Both vibrational modes still have similar intensities. However, the calculations do not explain the additional splitting of the symmetrical stretching mode absorbing weakly at  $\tilde{\nu} = 2075 \text{ cm}^{-1}$ .

NMR spectroscopy has been used for the characterization of isolable rhodium acyl complexes as well as of sufficiently populated intermediates formed during catalysis with high rhodium loadings applied.  $^{13}\text{C}$  NMR shifts for the carbonyl carbon atom range from  $\delta = 199.3 \text{ ppm}$  ( $^2J(\text{C},\text{Rh}) = 63.6 \text{ Hz}$ ), in pentamethylcyclopentadienyl rhodium(III)  $\beta$ -trimethylsilylpropionyl intermediates of intermolecular olefin hydroacylation to  $\delta = 235.4 \text{ ppm}$  ( $\tilde{\nu}(\text{CO}) = 1675(\text{s}), 1750 \text{ cm}^{-1}(\text{m})$ ) in dichloro and chelate complexes.<sup>[33]</sup> An acetyl complex of  $\text{Rh}^{\text{I}}$  bearing a tetrapod  $\text{NP}_3$  ligand could be prepared from the corresponding hydride acetyl  $\text{Rh}^{\text{III}}$  complex by reduction with  $\text{NaBH}_4$ . For this complex, a  $^1\text{H}$  NMR resonance at  $\delta = 2.03 \text{ ppm}$  (q,  $^4J(\text{H},\text{P}) = 2.7 \text{ Hz}$ ) was attributed to the acetyl methyl group, together with an IR band at  $\tilde{\nu} = 1575 \text{ cm}^{-1}$ .<sup>[34]</sup> Because of the low metal concentrations usually applied in rhodium-catalyzed hydroformylation, advantage is taken from labeling with  $^{13}\text{CO}$  for the direct detection of the quaternary acyl carbon atom by  $^{13}\text{C}$  NMR spectroscopy. Thus, acyl intermediates  $\text{Rh}^{13}\text{C}(\text{O})(\text{CH}_2)_2\text{Ph}$  were unambiguously detected in toluene at  $\delta = 234\text{--}235 \text{ ppm}$  with rhodium concentrations of  $21 \text{ mM}$  applied.<sup>[6e]</sup> The signal of the Rh-bound heptanoyl carbon became observable after CO versus  $^{13}\text{CO}$  exchange and slowing down the rate of intra- and intermolecular exchange processes in a combined IR and NMR spectroscopic study of 1-hexene hydroformylation.<sup>[6f]</sup> For hydroformylation catalysts modified by bulky monophosphites, acyl rhodium complexes so far have been investigated intensively only by FTIR spectroscopy.

For our NMR spectroscopic study of the Rh/TDTBPP/CO/ $\text{H}_2$ /3,3-dimethyl-1-butene system we used a modified 10 mm sapphire NMR tube allowing for precise control of head space pressure and ensuring gas saturation of the sample for the entire measurement.<sup>[35]</sup> To enhance the chance of detection of rhodium acyl complexes, the concen-

tration of the rhodium precursor [(acac)Rh(CO)<sub>2</sub>] was set to 2.5 mM, representing an eight-fold concentration compared to catalysis, in [D<sub>14</sub>]n-hexane. Partial pressures of H<sub>2</sub> and of CO, 0.25 and 3.75 MPa, respectively, were adjusted to slow down the hydrogenolytic aldehyde formation. The ratio Rh/TDTBPP/3,3-dimethylbut-1-ene was 1:20:360 with the olefin added directly to the mixture of catalyst precursor and monophosphite at room temperature. The first <sup>31</sup>P NMR spectrum recorded under an argon atmosphere after dissolving all components, besides the signal of free ligand at δ = 130.6 ppm, exhibited the sharp doublet of [(acac)Rh(CO)L] at δ = 118.4 ppm (*J*(P,Rh) = 293 Hz). Immediately after the syngas was added, the signal of the rhodium complex started to broaden, now indicating an equilibrium occurring between free and coordinated phosphite. After 2 h at room temperature, the rhodium-precursor-to-catalyst transformation and the beginning of the hydroformylation catalysis is observed. In the carbonyl region of the <sup>13</sup>C NMR spectrum peaks for dissolved CO (δ = 184.8 ppm) and acetylacetone (δ = 190.4 ppm), together with distinct amounts of 4,4-dimethylpentanal (δ = 198.3 ppm) and 2,3,3-trimethylbutanal (δ = 201.9 ppm, 9:1 ratio of aldehydes) are assigned. Within the subsequent hours a new broad phosphorus signal appeared at δ = 134.1 ppm (*d*, *J*(P,Rh) = 137 Hz), which shifted marginally and became sharper upon cooling to 241 K (δ = 135.5 ppm (*d*, *J*(P,Rh) = 125.4 Hz)) and permanently held 5% of signal intensity, pointing to the coordination of one phosphite to rhodium in this intermediate. The rhodium hydride complexes remained below the detection limits during a longer period of time, whereas large amounts of olefin were converted to aldehyde (47% within 16 h at 301 K). However, we were not able to detect signals for Rh-bound carbonyls or the acyl group by measuring long term as well as INEPT and HMBC <sup>13</sup>C-<sup>1</sup>H NMR spectra within the temperature range of 301 and 241 K, even at stopped syngas flow to further reduce the probability of acyl complex hydrogenolysis by dissolved H<sub>2</sub> (δ = 4.55 ppm). In the <sup>1</sup>H NMR spectra, the intense signals of the olefin caused severe overlaps. However, the appearance of a new broad triplet in the proton spectrum at δ = 2.69 ppm, assignable to rhodium acyl α-methylene protons,<sup>[36]</sup> was synchronized with the observation of the phosphorus signal at δ = 134.1 ppm and correlated to a less intense carbon resonance at δ = 38.8 ppm. These signals began to disappear after the olefin conversion reached 90% and signals, which compare to that of the known hydride complexes [HRh(CO)<sub>3</sub>(TDTBPP)] (δ = 136.7 ppm (*d*, *J*(P,Rh) = 250 Hz)) and [HRh(CO)<sub>2</sub>(TDTBPP)<sub>2</sub>] (δ = 134.3 ppm (*d*, *J*(P,Rh) = 226 Hz)) became detectable in a 1:1 ratio.<sup>[5d]</sup>

Interestingly, even at these high olefin conversions the acyl intermediate could be repopulated to be the predominant one simply by stopping the syngas flow in the NMR cell, thus slowing down hydrogenolysis and reformation of the rhodium hydride. Full olefin conversion within the NMR sample was achieved within four days with 91% selectivity in 4,4-dimethylpentanal. After depressurizing the NMR cell and purging the solution with argon, [HRh(CO)<sub>2</sub>(TDTBPP)<sub>2</sub>] remained as the only rhodium complex. Be-

cause the time-dependent concentration profiles for organic as well as metal-organic components as seen in the <sup>1</sup>H and <sup>31</sup>P NMR measurements do fit qualitatively to the results of our in situ FTIR study we conclude that the new proton signal observed at δ = 2.69 ppm belongs to [C<sub>6</sub>H<sub>13</sub>C(O)Rh(CO)<sub>3</sub>(TDTBPP)].<sup>[37]</sup>

## Conclusion

There are still a couple of interesting facets of olefin hydroformylation worth being studied. This also holds for the rhodium-catalyzed reaction, despite the fact that it is well established in both, industry and academia. Our work presented here does exemplify that in situ spectroscopy allows not only for the identification of organometallic intermediates, but also for a time-resolved determination of individual concentrations of components if the respective methodological prerequisites are met. The kinetic approach we applied takes benefit from the fact that data are available for the entire olefin conversion range. Rates at catalyst saturation became accessible by such kinetic analysis as well as further details as are the concentration of the catalyst substrate complex, and the value of the constant *k*<sub>2</sub><sup>obs</sup>. It was shown with the help of *K*<sub>m</sub> that the pre-equilibrium is not established, and therefore kinetic derivations based on the steady-state approximation are suitable for this reaction system. The rate-controlling step is dependent on the substrate concentration, but is always limited by hydrogenolysis. We conclude that the hydroformylation mechanism of the transition-metal catalytic system investigated in this paper is consistent with Michaelis–Menten-type kinetics. A further interesting result is the difference in the coordination site, equatorial versus axial, which is preferred by the phosphite ligand upon coordination at the saturated hydrido and acyl complexes, respectively. DFT calculations on these complexes did not reproduce all features of the experimental IR spectra in detail but do strongly support the initial assumptions of the respective assignments. Based on the results from DFT calculations and as further analyzed with the NBO theory, the origin of an additionally occurring asymmetric stretching vibration of the carbon monoxide ligands of the acyl complex is not a result of steric hindrance but of distinct orbital interactions. There are certainly more of such “hidden stories” to discover, which, complementary to literature data, will lead to a better understanding of this highly interesting type of catalyst.

## Experimental Section

**Materials:** 3,3-Dimethyl-1-butene (>99% (GC), Sigma–Aldrich, 95% was distilled over sodium and stored under argon. *n*-Hexane (Sigma–Aldrich, >99%) was distilled over Sicapent (Merck) and stored under argon. Dodecane (Sigma–Aldrich, >99%), which was used as internal GC-standard, was dried by storage over Sicapent for one week and distilled after separation of the drying agent and stored under argon. Fur-

ther chemicals used in this study: acetylacetonato dicarbonyl rhodium(I) (39.46 % Rh, Umicore), tri(2,4-di-*tert*-butylphenyl)phosphite (TDTBPP Sigma-Aldrich, 98 %). Gases used in this study: synthesis gas (CO/H<sub>2</sub> = 1:1, from carbon monoxide 99.997 % and hydrogen 99.999 %, Linde), carbon monoxide (99.997 %, Linde), hydrogen (99.9993 %, Linde), and argon (99.999 %, Linde).

As a phosphite stabilizer bis(2,2,6,6-tetramethyl-4-piperidyl)-sebacate (Tinuvin 770 DF, 100 %, Ciba) was added in equimolar amounts to the ligand.<sup>[11]</sup>

**Devices and procedures:** The HP FTIR apparatus for performing the hydroformylation reactions consisted of a 200 mL stainless steel autoclave with gas entrainment impeller and an oil bath thermostat (premix reactor AG, Leimen, Germany) equipped with a heatable transmission flow-through IR cell (Dr. Bastian Feinwerktechnik GmbH, Wuppertal, Germany) and an automated sampling device (ASD) for taking GC samples during the reaction (amplus GmbH, Rostock, Germany) (see Figure 14).

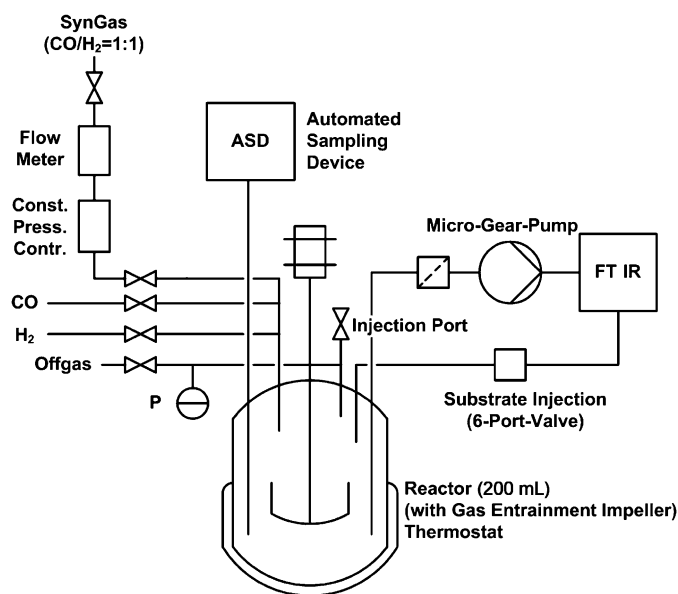


Figure 14. Scheme of the experimental HP FTIR apparatus equipped with an automated sampling device.

Circulation of the reaction solution through the IR cell and back to the autoclave was realized by a micro gear pump (mzr-7255, HNP Mikrosysteme GmbH, Parchim, Germany). A 6-port valve (Knauer GmbH, Berlin, Germany) with a 6.5 mL loop was used for olefin injection. A Bruker Tensor 27 FTIR spectrometer with a MCT-A detector was used. ZnS (Korth Kristalle GmbH, Kiel, Germany) was used as window material. The mean optical path length was 0.48 mm resulting from a wedged spacer. Pressurization facilities were installed for synthesis gas (CO/H<sub>2</sub> = 1:1) as well as hydrogen and carbon monoxide. For regulation of the consumed gas (CO/H<sub>2</sub> = 1:1) and keeping the pressure constant during the reaction a pressure controller (Brooks Instrument, Hatfield, PA, USA) was used. No mass transport limitation occurs with such experimental setup under the conditions applied.<sup>[11]</sup>

Solutions in *n*-hexane were prepared from the solids by using a syringe and Schlenk techniques. All components except the olefin were transferred into the autoclave. The stirrer speed was set to 1500 rpm, the speed of the micro-gear pump (displacement volume: 48  $\mu$ L) was set to 2333 rpm. After heating the solution to 30 °C the overhead pressure was about 0.15 MPa (argon, solvent vapor), the system was pressurized with 1 MPa carbon monoxide and the respective hydrogen partial pressure. After preformation of the hydrido complexes was complete, the olefin

was injected, and the FTIR measurements and the sampling procedure were started.

FTIR spectra were recorded between  $\tilde{\nu}$  = 3950 and 700 cm<sup>-1</sup> with a spectral resolution of 2 cm<sup>-1</sup>. Per FTIR spectrum ten scans were collected (double-sided, forward-backward) with a mirror speed set to 40 kHz. Intervals between two measurements were 37 s (for the first 120 min) and after that 67 s.

**Rapid scan measurements:** For these measurements the Bruker software tool OPUS-Chrom was used. The spectral resolution was set to 4 cm<sup>-1</sup>. One scan per spectrum was recorded (single-sided) with a delay time of 0.244 s between spectra at a mirror speed of 40 kHz.

As an internal reference for the investigation of the equilibrium between the hydrido complexes, the carbonyl band at  $\tilde{\nu}$  = 1740 cm<sup>-1</sup> of bis(2,2,6,6-tetramethyl-4-piperidyl)-sebacate has been used.

A 7890 A GC System from Agilent Technologies with a Petrocol DH 150 column (Supelco, Inc.) was used for GC analyses.

NMR spectra were obtained on a Bruker Avance 400 spectrometer by using a high-pressure gas flow cell connected to devices allowing for continuous gas supply and the control of gas flow and pressure.<sup>[35]</sup>

## Computational Details

Geometry optimization and frequency calculations were performed by using the Gaussian 03 and Gaussian 09 program packages.<sup>[38]</sup> For all calculations done we used the PBE exchange density functional, the PBE gradient-corrected correlation density functional and the DGDZVP basis set.<sup>[39]</sup> No imaginary frequencies were found, which indicates that the optimized structures are at least local minimum structures on the potential energy surface.

## Acknowledgements

We thank Evonik Industries AG for financial support. For helpful discussions and suggestions we especially thank Prof. Detlef Heller.

- [1] a) *Rhodium-Catalyzed Hydroformylation* (Eds.: P. W. N. M. van Leeuwen, C. Claver), Kluwer, Dordrecht, **2000**; b) K.-D. Wiese, D. Obst in *Topics in Organometallic Chemistry, Vol. 18* (Ed.: M. Beller), Springer, Heidelberg, **2006**.
- [2] *Mechanisms in Homogeneous Catalysis* (Ed.: B. Heaton), Wiley-VCH, Weinheim, **2005**.
- [3] a) M. Garland in *Mechanisms in Homogeneous Catalysis* (Ed.: B. Heaton), Wiley-VCH, Weinheim, **2005**, pp. 151–193; b) C. Li, E. Widjaja, M. Garland, *J. Catal.* **2003**, *213*, 126–134; c) J. Feng, M. Garland, *Organometallics* **1999**, *18*, 417–427; d) C. Li, E. Widjaja, M. Garland, *J. Am. Chem. Soc.* **2003**, *125*, 5540–5548; e) C. Li, L. Chen, M. Garland, *J. Am. Chem. Soc.* **2005**, *129*, 13327–13334.
- [4] a) W. Chew, E. Widjaja, M. Garland, *Organometallics* **2002**, *21*, 1982–1990; b) E. Widjaja, C. Li, M. Garland, *Organometallics* **2002**, *21*, 1991–1997; c) E. Widjaja, C. Li, W. Chew, M. Garland, *Anal. Chem.* **2003**, *75*, 4499–4507.
- [5] a) D. Evans, J. A. Osborn, G. Wilkinson, *J. Chem. Soc. A* **1968**, 3133–3142; b) C. K. Brown, G. Wilkinson, *J. Chem. Soc. A* **1970**, 2753–2764; c) T. Jongsmas, G. Challa, P. W. N. M. van Leeuwen, *J. Organomet. Chem.* **1991**, *421*, 121–128; d) R. Crous, M. Datt, D. Foster, L. Bennie, C. Steenkamp, J. Huyser, L. Kirsten, G. Steyl, A. Roodt, *J. Chem. Soc. Dalton Trans.* **2005**, 1108–1116.
- [6] a) M. Garland, P. Pino, *Organometallics* **1991**, *10*, 1693–1704; b) C. Fyhr, M. Garland, *Organometallics* **1993**, *12*, 1753–1764; c) G. Liu, R. Volken, M. Garland, *Organometallics* **1999**, *18*, 3429–3436; d) J. Zhang, M. Poliakoff, M. W. George, *Organometallics* **2003**, *22*, 1612–1618; e) J. M. Brown, A. G. Kent, *J. Chem. Soc. Perkin Trans.*

- 2 **1987**, 1597–1607; f) S. C. van der Slot, P. C. J. Kamer, P. W. N. M. van Leeuwen, J. A. Iggo, B. T. Heaton, *Organometallics* **2001**, *20*, 430–441.
- [7] a) C. Godard, S. B. Duckett, S. Polas, R. Tooze, A. C. Whitwood, *Dalton Trans.* **2009**, 2496–2509; b) C. Godard, S. B. Duckett, S. Polas, R. Tooze, A. C. Whitwood, *J. Am. Chem. Soc.* **2005**, *127*, 4994–4995; c) L. Damoense, M. Datt, M. Green, C. Steenkamp, *Coord. Chem. Rev.* **2004**, *248*, 2393–2407; d) C. Godard, S. B. Duckett, C. Henry, S. Polas, R. Tooze, A. C. Whitwood, *Chem. Commun.* **2004**, 1826–1827.
- [8] a) A. B. Permin, R. Eisenberg, *J. Am. Chem. Soc.* **2002**, *124*, 12406–12407; b) P. P. Deutsch, R. Eisenberg, *Organometallics* **1990**, *9*, 709–718; c) L. Versluis, T. Ziegler, *Organometallics* **1990**, *9*, 2985–2992; d) M. Solà, T. Ziegler, *Organometallics* **1996**, *15*, 2611–2618; e) T. Matsubara, N. Koga, Y. Ding, D. G. Musaev, K. Morokuma, *Organometallics* **1997**, *16*, 1065–1078; f) M. Torrent, M. Solà, G. Frenking, *Chem. Rev.* **2000**, *100*, 439–493.
- [9] Unsaturated complexes have been observed under non-catalytic conditions only. a) D. Evans, G. Yagupsky, G. Wilkinson, *J. Chem. Soc. A* **1968**, 2660–2665; b) R. V. Kastrup, J. S. Merola, A. A. Oswald, *Adv. Chem. Ser.* **1982**, No. 196, Chapter 3; c) M. A. Freeman, D. A. Young, *Inorg. Chem.* **1986**, *25*, 1556–1560. For an 16-electron acyl complex of iridium(I) see: G. Yagupsky, C. K. Brown, G. Wilkinson, *J. Chem. Soc. A* **1970**, 1392–1401.
- [10] a) P. C. J. Kamer, J. N. H. Reek, P. W. N. M. van Leeuwen in *Mechanism in Homogeneous Catalysis* (Ed.: B. Heaton), Wiley-VCH, Weinheim, **2005**, pp. 231–269; b) E. Zuidema, L. Escorihuela, T. Eichelsheim, J. J. Carbó, C. Bo, P. C. J. Kamer, P. W. N. M. van Leeuwen, *Chem. Eur. J.* **2008**, *14*, 1843–1853; c) A. van Rooy, P. C. J. Kamer, P. W. N. M. van Leeuwen, K. Goubitz, J. Fraanje, N. Veldman, A. L. Spek, *Organometallics* **1996**, *15*, 835–847; d) P. C. J. Kamer, A. van Rooy, G. C. Schoemaker, P. W. N. M. van Leeuwen, *Coord. Chem. Rev.* **2004**, *248*, 2409–2424; e) A. van Rooy, E. N. Orij, P. C. J. Kamer, F. van den Aardweg, P. W. N. M. van Leeuwen, *J. Chem. Soc. Chem. Commun.* **1991**, 1096–1097; f) A. van Rooy, E. N. Orij, P. C. J. Kamer, P. W. N. M. van Leeuwen, *Organometallics* **1995**, *14*, 34–43; g) A. van Rooy, J. N. H. de Bruijn, K. F. Roobek, P. C. J. Kamer, P. W. N. M. van Leeuwen, *J. Organomet. Chem.* **1996**, *507*, 69–73.
- [11] C. Kubis, R. Ludwig, M. Sawall, K. Neymeyr, A. Börner, K.-D. Wiese, D. Hess, R. Franke, D. Selent, *ChemCatChem* **2010**, *2*, 287–295.
- [12] A. A. Dabbawala, H. C. Bajaj, R. V. Jasra, *J. Mol. Catal. A* **2009**, *302*, 97–106.
- [13] H.-J. Drexler, A. Preetz, T. Schmidt, D. Heller in *The Handbook of Homogeneous Hydrogenation* (Eds.: J. G. de Vries, C. J. Elsevier), Wiley-VCH, Weinheim, **2007**, pp. 257–293.
- [14] C. Bergounhou, D. Neibecker, R. Mathieu, *J. Mol. Catal. A* **2004**, *220*, 167–182.
- [15] a) F. G. Hellferich, *Kinetics of Homogeneous Multistep Reactions in Comprehensive Chemical Kinetics, Vol. 38*, 2nd ed. (Ed.: N. J. B. Green), Elsevier, Amsterdam, **2004**; b) J. H. Espenson in *Encyclopedia of Catalysis, Vol. 4* (Ed.: I. T. Horváth), Wiley, New York, **2003**, pp. 490–508; c) D. G. Blackmond, *Angew. Chem.* **2005**, *117*, 4374–4393; *Angew. Chem. Int. Ed.* **2005**, *44*, 4302–4320; d) D. Murzin, T. Salmi, *Catalytic Kinetics*, Elsevier, Amsterdam, **2005**.
- [16] J. W. Rathke, R. J. Klingler, T. R. Krause, *Organometallics* **1991**, *10*, 1350–1355.
- [17] J. A. Christiansen, *Adv. Catal.* **1953**, *5*, 311–353.
- [18] E. J. King, C. Altman, *J. Phys. Chem.* **1956**, *60*, 1375–1378.
- [19] See the Supporting Information, SI-B, for plots of the GC data.
- [20] a) See the Supporting Information, SI-C, for results of the simulation of the Michaelis–Menten mechanism and the following integration/regression procedure; b) K. J. Laidler, *Can. J. Chem.* **1955**, *33*, 1614–1624.
- [21] K. Neymeyr, M. Sawall, D. Hess, *J. Chemom.* **2010**, *24*, 67–74.
- [22] Otherwise a successful factorization appeared to be impossible. To get rid of these perturbing signals we used a separate spectrum of the background at the reaction conditions, and also a separate spectrum of the background including 3,3-dimethyl-1-butene. The zero lines of the spectra were corrected. By computing the difference between these two spectra we obtained an approximation of the olefin spectrum. Furthermore the concentration profile of the olefin (during the hydroformylation process) was accessible from a flank of the C=C valence vibration band at  $\tilde{\nu}=1646.8\text{ cm}^{-1}$ . The computed olefin spectrum was multiplied with the olefin concentration and then subtracted from the zero-line-corrected series of spectra obtained from the hydroformylation reaction solution.
- [23] a) A. de Juan, M. Maeder, M. Martínez, R. Tauler, *Chemom. Intell. Lab. Syst.* **2000**, *54*, 123–141; b) H. Haario, V.-M. Taavitsainen, *Chemom. Intell. Lab. Syst.* **1998**, *44*, 77–98.
- [24] For the details on the mathematical algorithm and the optimization procedure see: M. Sawall, A. Börner, C. Kubis, R. Ludwig, D. Selent, K. Neymeyr, unpublished results.
- [25] K. J. Laidler, *J. Chem. Educ.* **1988**, *65*, 250–254.
- [26] E. Brunner, *J. Chem. Eng. Data* **1985**, *30*, 269–273. Comment: solubility data for hydrogen in *n*-hexane were available for  $T=298.15$ ,  $323.15$ , and  $373.15\text{ K}$ . We calculated the solubility for our reaction temperature of  $303.15\text{ K}$  as follows: for each temperature mole fractions for respective partial pressures of hydrogen were obtained from linear regression. By  $\ln(x)=A/T+B$ , mole fractions for  $303.15\text{ K}$  were calculated for each partial pressure.
- [27] See the Supporting Information (SI-D), for a presentation of the graphs obtained from the fitting process for each hydrogen concentration applied.
- [28] For the full set of concentration profiles as well as a table containing the values of  $k_2^{\text{obs}}$  and  $K_m$ , which were determined for different hydrogen pressures, see the Supporting Information (SI-E).
- [29] R. Koelliker, H. Thies, *J. Chem. Eng. Data* **1993**, *38*, 437–440. We calculated the solubilities for our reaction temperature at  $303.15\text{ K}$  the same way as in reference [23] from the data for  $T=293.15$ ,  $323.15$ , and  $373.15\text{ K}$ .
- [30] a) A. D. Allian, Y. Wang, M. Saeys, G. M. Kuramshina, M. Garland, *Vibrational Spectroscopy* **2006**, *41*, 101–111; b) A. D. Allian, M. Tjahjono, M. Garland, *Organometallics* **2006**, *25*, 2182–2188; c) A. Christiansen, C. Li, M. Garland, D. Selent, R. Ludwig, R. Franke, A. Börner, *ChemCatChem* **2010**, *2*, 1278–1285; d) A. Christiansen, C. Li, M. Garland, D. Selent, R. Ludwig, A. Spannenberg, W. Baumann, R. Franke, A. Börner, *Eur. J. Org. Chem.* **2010**, 2733–2741; e) A. Boddien, B. Loges, F. Gärtner, C. Torborg, K. Fumino, H. Junge, R. Ludwig, M. Beller, *J. Am. Chem. Soc.* **2010**, *132*, 8924–8934; f) F. Gärtner, A. Boddien, E. Barsch, K. Fumino, S. Losse, H. Junge, D. Hollmann, A. Brückner, R. Ludwig, M. Beller, *Chem. Eur. J.* **2011**, *17*, 6425–6436; g) D. Selent, R. Franke, C. Kubis, A. Spannenberg, W. Baumann, B. Kreidler, A. Börner, *Organometallics* **2011**, *30*, 4509–4514.
- [31] a) P. C. Ford, S. Massick, *Coord. Chem. Rev.* **2002**, *226*, 39–49; b) S. M. Massick, J. G. Rabor, S. Elbers, J. Marhenke, S. Bernhard, J. R. Schoonover, P. C. Ford, *Inorg. Chem.* **2000**, *39*, 3098–3106; c) J. Somlyai-Haász, F. Haáz, V. Galamb, A. Benedetti, C. Zucci, G. Pályi, T. Krümming, B. Happ, T. Bartik, *J. Organomet. Chem.* **1991**, *419*, 205–217; d) I. Kovács, F. Ungváry, *Coord. Chem. Rev.* **1997**, *161*, 1–32.
- [32] a) NBO Version 3.1, E. D. Glendening, A. E. Reed, J. E. Carpenter, F. Weinhold; b) A. E. Reed, L. A. Curtiss, F. Weinhold, *Chem. Rev.* **1988**, *88*, 899–926; c) F. Weinhold, C. R. Landis, *Valency and Bonding*, Cambridge University Press, Cambridge, **2005**. See the Supporting Information, SI-G, for a detailed description of the analysis.
- [33] a) A. H. Roy, C. P. Lenges, M. Brookhart, *J. Am. Chem. Soc.* **2007**, *129*, 2082–2093; b) G. L. Moxham, H. Randell-Sly, S. K. Brayshaw, A. S. Weller, M. Willis, *Chem. Eur. J.* **2008**, *14*, 8383–8397; c) J. A. Miller, J. A. Nelson, *Organometallics* **1991**, *10*, 2958–2961; d) M. A. Garralda, R. Hernández, L. Ibarlucea, E. Pinilla, M. R. Torres, M. Zarandona, *Organometallics* **2007**, *26*, 1031–1038.
- [34] C. Bianchini, A. Meli, M. Peruzzini, F. Vizza, F. Bachechi, *Organometallics* **1991**, *10*, 820–823.
- [35] D. Selent, W. Baumann, A. Börner (LIKAT e.V.), DE 10333143, 17.07., **2003**.

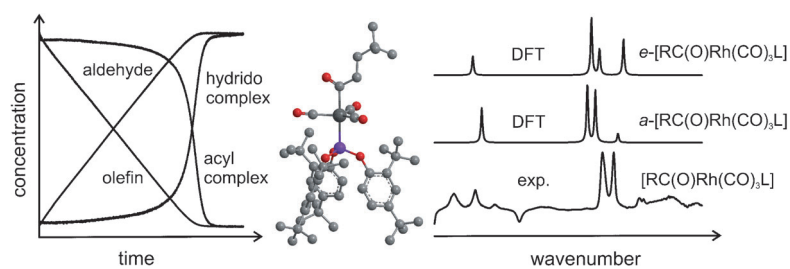
- [36] In  $[\text{CH}_3\text{CH}_2\text{C}(\text{O})\text{Ir}(\text{dppe})(\text{CO})]$  (dppe = 1,2-bis(diphenylphosphino)ethane), the propionyl methylene protons resonate at  $\delta = 2.83$  ppm ( $\tilde{\nu} = 1635 \text{ cm}^{-1}$ ), see reference [8b].
- [37] See the Supporting Information, SI-G, for a selection of spectra.
- [38] a) Gaussian 03, Revision D.01, M. J. Frisch et al. Gaussian Inc., Wallingford CT, **2004**; b) Gaussian 09, Revision A.1, M. J. Frisch et al. ; Gaussian Inc., Wallingford CT, **2009**. For the complete list of authors see the Supporting Information, SI-H.
- [39] a) J. P. Perdew, K. Burke, M. Ernzerhof, *Phys. Rev. Lett.* **1996**, *77*, 3865–3868; b) J. P. Perdew, K. Burke, M. Ernzerhof, *Phys. Rev. Lett.* **1997**, *78*, 1396; c) N. Godbout, D. R. Salahub, J. Andzelm, E. Wimmer, *Can. J. Chem.* **1992**, *70*, 560–571; d) C. Sosa, J. Andzelm, B. C. Elkin, E. Wimmer, K. D. Dobbs, D. A. Dixon, *J. Phys. Chem.* **1992**, *96*, 6630–6636.

Received: February 23, 2012  
Published online: ■ ■ ■, 2012

**Catalysis**

C. Kubis, D. Selent,\* M. Sawall,  
R. Ludwig, K. Neymeyr, W. Baumann,  
R. Franke, A. Börner..... ■■■■-■■■■

**Exploring Between the Extremes:  
Conversion-Dependent Kinetics of  
Phosphite-Modified Hydroformylation  
Catalysis**



**Catalyst at work:** Organic as well as organometallic components have been followed by FTIR spectroscopy during the rhodium-catalyzed hydroformylation. All concentration profiles obtained fit to Michaelis–Menten-type kinetics. The pre-equilibrium towards

the acyl complex intermediate is not established. Spectroscopic and results from DFT calculations show that the coordination mode of the phosphite in the acyl complex is different from that in the corresponding hydride (see figure).